

Study of mass and CM position impact on a ship's hull resistance

FINAL REPORT FOR AERODYNAMICS OF TRANSPORT VEHICLES

Nil Couto Ovejero, 10778438

Clara Rondeau Gómez, 10836370

Lecturer:

Prof. Luigi Vigevano
Prof. Paolo Schito

1. Problem Definition

The main objective of this study is to predict ship resistance while varying the mass and center of gravity position of a container ship. The geometry used is the Duisburg Test Case, a 14000TEU post-Panamax container vessel [4]. The geometry is shown in Figure 1.

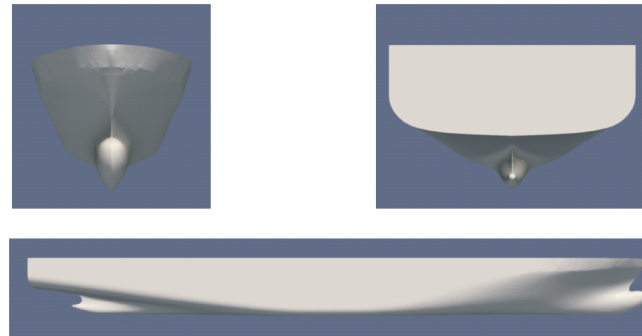


Figure 1: Bow view, stern view and side view of DTC

The results obtained could be applied for future trimming of boats towards the reduction of fuel consumption. In order to analyse the performance of the hull, two masses will be considered: one representing a normal-loaded condition of the ship ($14000 \text{ TEU} \approx 330000 \text{ kg}$), while the second one represents a high-loaded limiting case ($17000 \text{ TEU} \approx 410000 \text{ kg}$), where $1 \text{ TEU} \approx 23600 \text{ kg}$. The mass of the simulated models are 412.57 kg and 512.95 kg respectively. Note that these masses correspond to half of the ship model. In addition, 3 centers of masses positions [CM] will be considered (Table 1): a centered condition with the CM at half of the ship length, one with the CM placed 5% of the total hull's length forward of the centered condition and one with the CM placed 5% behind of the centered condition. Note that the CM positions studied just vary in the x-direction, and they are always placed in the symmetry plane of the hull ($y = 0$). Therefore, the present project focuses on longitudinal dynamics only and its effect on the hull's resistance.

Other configurations have been simulated in order to find the limiting cases. As it can be seen in Figure 2, a 10% displacement on the mass center was applied (both forward and backward) obtaining critical conditions, mainly in the forward configuration where the bow is completely sunk in the water.

Table 1: Different positions of the CM at (x, y, z) [m]

	Full-Scale	Model
Forward	(138.53, 0, 11.88)	(2.33191, 0, 0.2)
Centered	(175.7853, 0, 11.88)	(2.929, 0, 0.2)
Behind	(209.5368, 0, 11.88)	(3.527141, 0, 0.2)

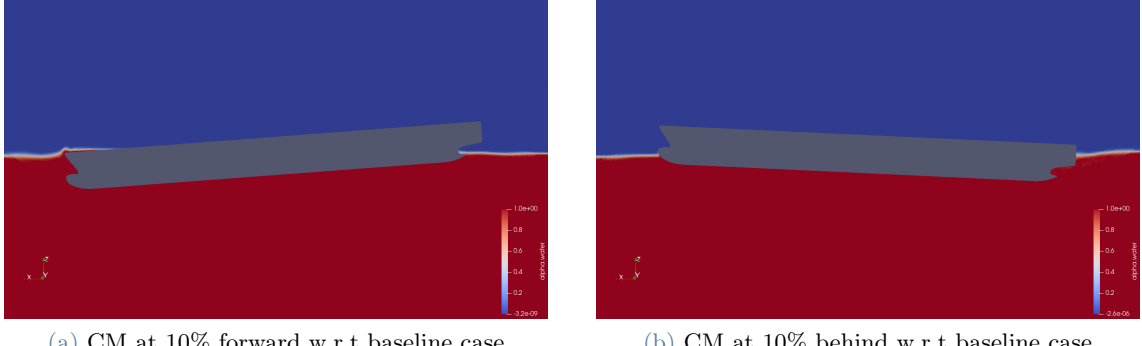


Figure 2: Limiting cases for the displacement of the CM

The main characteristics and parameters of the full scale and model ship are given in Table 2, where L_{pp} is the length between perpendiculars, B the breadth, T the draft, S_w the wetted surface, V the volume displacement and C_b the block coefficient.

Table 2: Main characteristics of DTC [4]

	Ship	Model
L_{pp} [m]	355	5.976
B [m]	51	0.429
T [m]	14.5	0.244
V [m^3]	173467	0.827
C_b [-]	0.661	0.661

1.1. Theoretical Background

1.1.1 Governing Equations

The Navier-Stokes equations for incompressible flow take the form:

$$\frac{\partial u_i}{\partial x_i} = 0 \quad (1)$$

$$\frac{\partial u_i}{\partial t} + \frac{\partial u_i u_j}{\partial x_j} = -\frac{1}{\rho} \frac{\partial p}{\partial x_i} + \nu \frac{\partial^2 u_i}{\partial x_j \partial x_j} \quad (2)$$

Substituting each variable ϕ by the average $\bar{\phi}$ and fluctuation ϕ' terms: $\phi = \bar{\phi} + \phi'$

Being $\phi(x, t)$ a generic flow variable, it can be written as the sum of its mean ($\bar{\phi}(x, t)$) and fluctuating components ($\phi'(x, t)$), $\phi(x, t) = \bar{\phi}(x, t) + \phi'(x, t)$, then substituting it in the Navier-Stokes equations and taking the time average results in the following Reynolds-averaged Navier-Stokes equations (RANS),

$$\frac{\partial \bar{u}_i}{\partial x_i} = 0 \quad (3)$$

$$\frac{\partial \bar{u}_i}{\partial t} + \frac{\partial \bar{u}_i \bar{u}_j}{\partial x_j} = -\frac{1}{\rho} \frac{\partial \bar{p}}{\partial x_i} + \nu \frac{\partial^2 \bar{u}_i}{\partial x_j \partial x_j} - \frac{\partial \bar{u}'_i \bar{u}'_j}{\partial x_j} \quad (4)$$

where the term $\overline{u'_i u'_j}$ is the Reynolds stress tensor denoted by R_{ij} and was approximated using Boussinesq hypothesis. When dealing with turbulence modeling, this term was modeled with Menter's Shear Stress Transport model, also known as SST turbulence model. As simulations are going to be unsteady, URANS will be used instead of the normal RANS equations.

1.1.2 Two-phase Flow

Note that the problem tackled implies a two-fluid interaction (air and water), and from a numerical point of view this is not straightforward [1]. Thus, a rearrangement of the governing equations needs to be made. In a two-phase flow, apart from solving the basic single-phase problem, the interface's location and its evolution in time should be also solved. The *one-fluid model* is the most used one by assuming continuity across the interface where all fields have been defined in both phases. In order to differentiate both phases, the volume fraction α has to be introduced where $\alpha = 0$ stands for only air inside the cell, and $\alpha = 1$ is completely immersed in water. In theory, when there is an abrupt change in α from 0 to 1 means that a change in phase has occurred, but depending on the model chosen it is more or less complicated to obtain such a sharp interface: usually, there are a certain number of cells that define the free surface where α varies continuously from 0 to 1. When working with numerical ship simulations, the computation of the free surface is really important as the interface coincides with the wave pattern, which has a main role in the total drag. Thus, the density, dynamic viscosity, and velocity fields are defined as follows:

$$\rho = \alpha \rho_1 + (1 - \alpha) \rho_2 \quad (5)$$

$$\nu = \alpha \nu_1 + (1 - \alpha) \nu_2 \quad (6)$$

$$U = \alpha U_1 + (1 - \alpha) U_2 \quad (7)$$

These new variables can be introduced into the RANS equations from Section 1.1.1.

1.1.3 Similarity Laws for model Tests

When estimating the hull's drag, results can be obtained through statistical, experimental, or numerical approaches. The most common option is the numerical one based on CFD simulations. Nevertheless, experimental tests are fundamental both to develop an empirical or statistical method and to validate a CFD analysis. That's why a relationship between a full-scale hull (s) and the model (m) through a proportionality factor is required.

- Geometric similarity:

$$L_s = \lambda L_m \quad A_s = \lambda^2 A_m \quad V_{diss_s} = \lambda^3 V_{diss_m} \quad (8)$$

- Kinematic similarity:

$$t_s = t_m \quad V_s = \lambda V_m \quad (9)$$

- Dynamic similarity:

Here, it is necessary to introduce the *Froude number*, which relates the inertia and gravity forces. If the full-scale ship and the model have the same Fr number, the dynamical similarity is ensured and the wave pattern will be geometrically similar.

$$Fr = \frac{V}{\sqrt{gL}} \quad (10)$$

Another well-known adimensional constant is the Reynolds number:

$$Re = \frac{VL}{\nu} \quad (11)$$

Equation 11 relates inertial and frictional forces. Therefore, if Re number is constant for both model and ship, the dynamical similarity is ensured.

In order to fulfill the first condition (Fr number), if the model is X times smaller than the real hull, it is sufficient to reduce the model's velocity by a scale of \sqrt{X} . On the contrary, to fulfill Reynold's Law with the same geometrical scale factor of X , the model's velocity would have to be X times larger, which is not feasible. So, in order to deal with this, tests are performed with the same Fr number, but not the same Re.

1.1.4 Ship's Resistance

Ships experience high levels of drag due to water and air effects, but its main contribution comes from *calm water resistance*. This kind of drag can be studied following two paths: as forces acting on the hull (friction and pressure resistance), or as a mechanism of energy dissipation (viscous and wave resistance).

- Forces acting on the hull:

The normal component of the hydrodynamic forces over the hull's surface is called *Pressure Resistance*, which comes from the hull's wave-making and viscous pressure. Instead, *frictional resistance* can be seen as the tangential component, that is due to the viscosity of the fluid.

- Mechanisms of energy dissipation:

The appearance of a wake behind the ship and the growth of the boundary layer around the surface due to viscous effects make the energy dissipate, so it can be seen as *viscous resistance*. *Wave resistance* comes from the lost power when generating wave patterns along the hull, where the pressure field acting on the immersed body causes a change in the water level and, as a result, the appearance of this pattern.

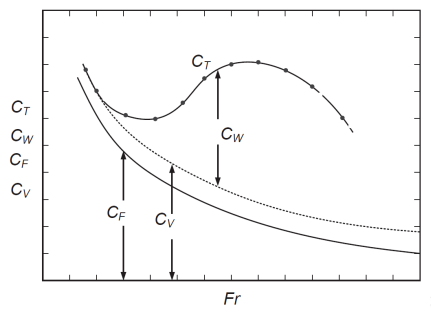


Figure 3: Resistance as a function of the Froude number

On the above plot (Figure 3), C_T is the total drag coefficient, C_W the wave resistance coeff., C_F is the friction resistance coeff and C_V the viscous resistance. It can be seen that the main components are the frictional and wave drag. The first one depends on the Reynolds number, hence the fluid velocity and characteristic length, so the hull's shape does not have any influence over this kind of drag. Instead, the wave-making component is bounded to the geometry, therefore, in order to reduce this type of resistance modifications to the hull's shape must be done.

The wave pattern generated by the motion of the ship consists of 2 wave systems:

- The motion of a ship through the water makes the pressure field vary, causing an increase or decrease in the height of the free surface, known as the *primary wave system*. This kind of wave strongly depends on the hull's shape, and not that much on the ship's velocity.
- *Secondary wave system*: It is composed of transverse and divergent waves which propagate downstream bounded by an angle $\alpha = 19,5$ (Kelvin wave pattern, Figure 4). This pattern is due to the superposition of many Kelvin waves which are produced by geometry discontinuities of the hull and interfere with each other.

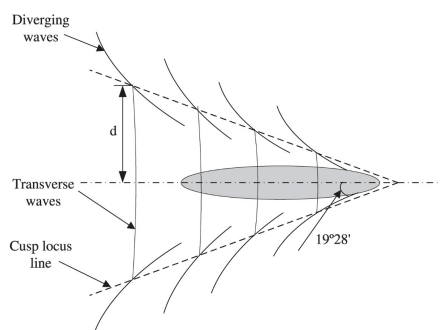


Figure 4: Kelvin wave

In short, if the ship wave pattern is high it will cause an increase of the wave drag. Waves tend to become higher with a high ship's velocity, but this tendency is not monotonically as it may appear a wave superposition effect.

2. Computational Model

All the simulations done in the present study have been performed using OpenFOAM with the interFoam solver and SST turbulence model [3]. A brief description of the solver has been presented in Section 2.2. In addition, given the large computational requirements to simulate 3D multi-phase unsteady cases, Amazon Elastic Compute Cloud (also known as Amazon EC2) services has been used. The usage of external servers was motivated by the fact that our personal computers were not powerful enough to deal with the requirements of the project in terms of computational power and time limitations.

2.1. Problem geometry and setup

The geometry of the DTC-Hull used has been presented before in Figure 1. Note that only half of the hull has been simulated, and symmetry boundary conditions have been exploited with the objective of saving computational resources. The model used to perform the simulations has been scaled by a ratio of 1:59,407. Some assumptions have to be made to simplify the problem at hand: calm water, no propeller, fixed trim condition and constant fluid (air and water) properties. Freestream conditions are presented in Table 3. Knowing that the velocity of the full-scale ship is $U = 12,86m/s = 25kn$ which corresponds to a Froude number of $Fr = 0,218$, hence, the velocity of the model is $U = 1,668m/s$ making use of that same Froude number.

Table 3: Freestream conditions

Velocity	1.668 m/s
Air density	1.225 kg/m^3
Water density	998.8 kg/m^3
Air kinematic viscosity	$1.48 \times 10^{-5} kg/m \cdot s$
Water kinematic viscosity	$1.09 \times 10^{-6} kg/m \cdot s$
Froud Number	0.218
Temperature	288.15K

Regarding the numerical domain used, a deep water condition is required for the solutions to be domain-independent. The computational domain is defined in `blockMeshDict`, where 6 blocks are created (Figure 5a). The interface is located at $z = 0.244$ m. Once, the `blockMesh` is executed, 42 cells along the x-axis and 19 cells along the y-axis are created, with a total of 134064 elements. Then, the `topoSet` and `refineMesh` are executed, whose purposes are to refine the mesh in the zone where the hull geometry will be placed by splitting the domain into 6 boxes (Figure 5b), after this process the mesh has 513216 cells.

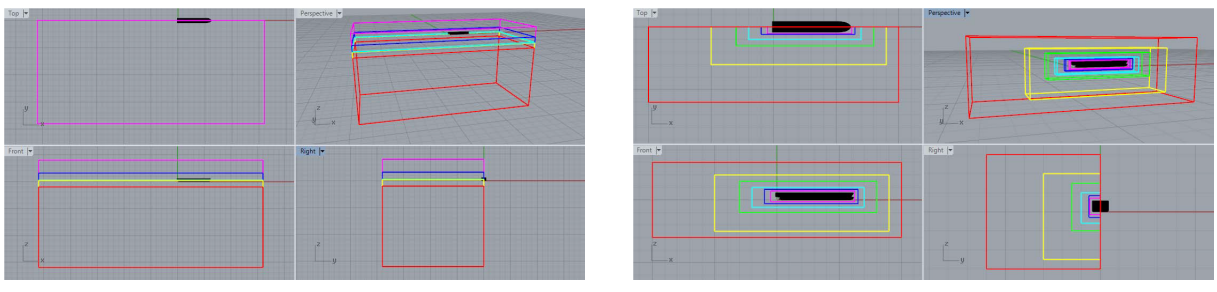


Figure 5: Division of the Domain

Lastly, when applying `snappyHexMesh`, the total number of cells increases up to 848025 elements. In this last process, the hull geometry is inserted into the mesh (extracted from the `stl` file) along with the different refined boxes. From here, the *snapping process* begins by refining the region and cells close to the hull's surface in order to capture the boundary layer effects. At this point, the mesh is ready, but in order to verify its quality `checkMesh` is used. Note that the process described corresponds to the generation of the fine grid. The modifications performed to generate the different meshes studied during the Mesh Independence Test are described in Section 2.3.

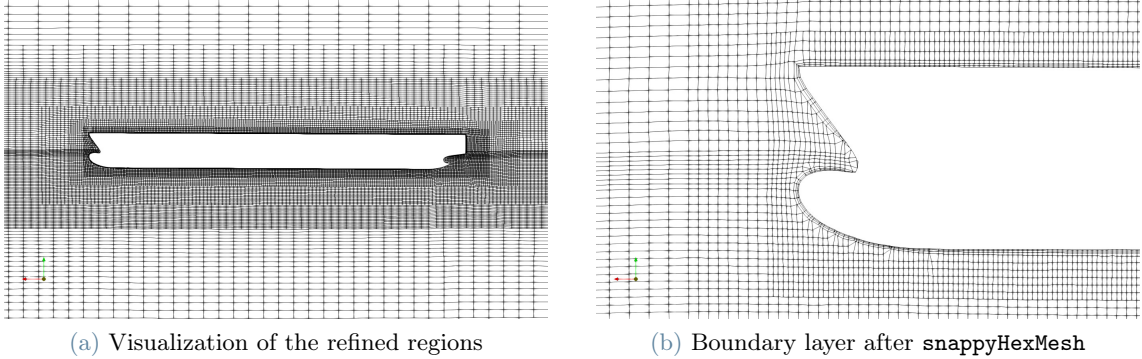


Figure 6: Final mesh

Boundary Conditions have been declared following [2]: seven patches have been defined as boundaries: inlet, outlet, bottom, atmosphere, side, midPlane and hull. The conditions for the inlet, outlet, and atmosphere are based on the velocity of the ship. Notice that the velocities for the portion of air and water are the same. For the hull, a no-slip wall condition is set both in water and air. Lastly, bottom, side and midPlane boundaries are set as symmetry planes.

2.2. Free-surface modelling

As mentioned previously, all simulations have been done using the InerFoam solver of OpenFoam [3], which is used when working with two incompressible, isothermal, immiscible fluids.

In order to compute the interface, Volume of Fluid method (VoF) has been used using the theory explained in Section 1.1.1. With this method, the volume fraction is defined as a function of the phase field: $\alpha(\phi) = 0,5(sgn(\phi) + 1)$. Where $sgn(\phi)$ is the signum function. Usually, compressive schemes are used due to numerical instabilities while reconstructing the free surface.

2.3. Mesh Independence Test

In order to validate the model presented and the future results, a Mesh Independence Test will be carried out. This test has the objective of obtaining a solution independent of the grid resolution while minimizing the computational resources required.

For the mesh independence study, three different meshes have been generated. One based on the parameters described in Section 2.1 (fine), and two more coarse cases:

- **Coarse:** The *snapping process* has been slightly modified by not adding layers near the wall. Thus, the `addLayers` option was disabled. Also, the number of divisions of the refined boxes near the hull geometry is reduced, obtaining a total of 582312 cells.
- **Medium:** The same reduction on the *snapping process* has been only done by disabling the `addLayers` option, obtaining a total of 766876 cells.
- **Fine:** The baseline case (tutorial case) has been used with no modifications in its parameters, with a total of 848025 cells.

Given the limited number of pages of the project, only a picture of the fine mesh has been presented in Figure 6.

In order to select a mesh to perform the subsequent studies, it has to be verified that the results have converged. This is because the criteria to compare the different grids is based on contrasting the relative error for the mean lift and drag coefficients obtained for the last 10 seconds of the simulations (thus, considered as converged values). The residuals of the volume fraction α have been analyzed and a total computational time of 30s has been considered as sufficient to have converged values. This can be also seen in Section 3.2, where the forces computed present periodic values for the last 10 seconds of the simulations approximately.

The relative errors between C_L and C_D for the coarse and medium grids with respect to the fine grid are presented in Table 4. Note that the simulations have been performed following the baseline case conditions, therefore the centered normal loading configuration:

Table 4: Mesh Independence Test results

	Coarse	Medium	Fine
Number of cells	582312	766876	848025
Relative error C_L [%]	0.007	0.0068	-
Relative error C_D [%]	17.473	10.455	-

From Table 4, it can be seen how the relative errors for C_L are very low for the 3 meshes considered. A large relative error on C_D is observed for both Coarse and Medium grids. These results suggest that a denser grid than the one it has been considered as Fine should have been studied since it cannot be stated that the Fine grid presents a solution independent of the mesh resolution. However, the Fine mesh studied is the one used in the OpenFOAM tutorial of the DTC-Hull, and in fact, this tutorial defines the baseline case of this study. For this reason, given that the tutorial has been considered as a validated case and that the computational power required for the Fine mesh is already very demanding, the Fine mesh has been considered as correct and it's been used for the subsequent studies.

3. Results

In this section, the results obtained for the different configurations are presented and discussed. Note that the simulations have been performed for a computational time of 30 seconds, time for which the residuals present a periodic behaviour as anticipated in Section 2.3.

3.1. Performance comparison

The performance comparison in terms of lift and drag coefficients is presented in Table 5. Note that the total lift and drag dimensional quantities presented account for the whole ship, and therefore they are twice the results obtained for the half hull simulated. The force coefficients have been computed as follows:

$$C_L = \frac{L_T}{\frac{1}{2}\rho_\infty U_\infty^2 S_w} \quad C_D = \frac{D_T}{\frac{1}{2}\rho_\infty U_\infty^2 S_w}$$

Where L_T and D_T are the total lift and drag forces respectively, ρ_∞ the water free-stream density, U_∞ the water free-stream velocity and S_w the wetted surface. Note that the wetted surface has to be assessed for each configuration.

Table 5: Performance comparison

	Loaded			Heavily Loaded		
	Forward	Centered	Behind	Forward	Centered	Behind
Wetted Surface [m^2]	6.57432	6.32745	6.42725	7.10264	7.0882	6.98199
Total Lift [N]	8098.7373	8098.0481	8098.6951	10124.3678	10122.8498	10122.1400
Total Drag [N]	35.5922	30.0092	39.3558	47.2865	39.4632	48.2752
Lift coefficient	0.8223	0.9211	0.9069	1.1516	1.0278	1.0434
Drag coefficient	0.0036	0.0034	0.0044	0.0054	0.0040	0.0050

Observing Table 5, it can be seen how the Forward configuration always shows the largest wetted surface. However, this doesn't have a direct impact on the total drag, since the largest dimensional resistance value corresponds to the Behind condition for both the Loaded and Heavily Loaded cases. This, combined with the fact that the Behind condition has lower wetted area than the other two CM configurations, results in the Behind configuration presenting the largest C_D values for the Loaded cases. The most penalizing condition in terms of drag coefficient is the Heavily Loaded Forward configuration. This case presents the larger wetted surface, for which both pressure and viscous force components acting against the boat motion are acting for a larger portion of the hull, resulting in a large C_D . This phenomenon can be related to the generation of the wave pattern that propagates downstream as explained in Section 1.1.4. Regarding the Centered condition, the Total Drag and C_D present the lowest values among the different CM positions, for both loading conditions. A more detailed reasoning of these results is presented in Section 3.2, where both lift and drag have been decomposed into their viscous and pressure components.

3.2. Lift and Drag components

A decomposition of total lift and drag into viscous and pressure components are presented in Figures 7 & 8:

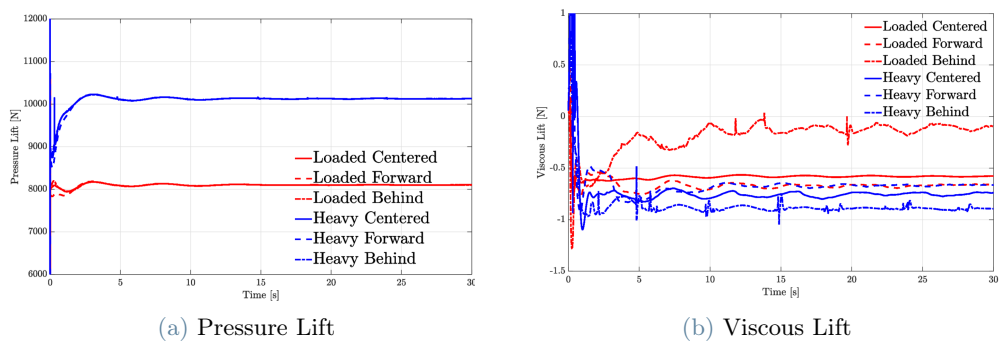


Figure 7: Lift components

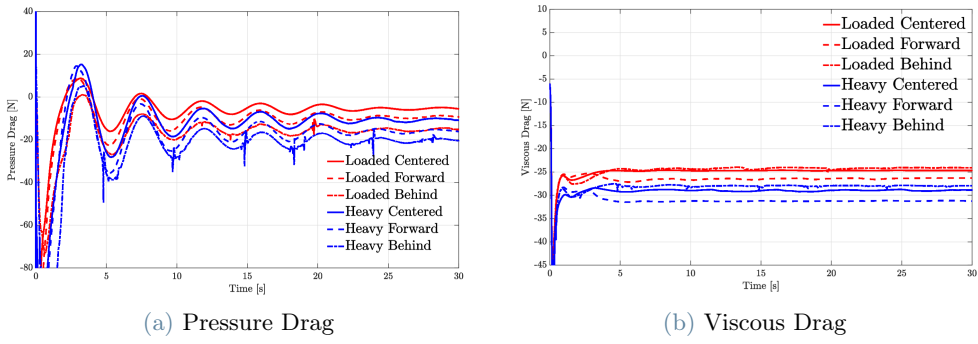


Figure 8: Drag components

It can be seen that for the heavily loaded case, there's an increase of the pressure lift w.r.t the loaded case (Figure 7a), as it is directly related to the weight's ship due to Buoyancy Forces (Archimedes' Principle) and not that much with the position of the CM. Concerning the viscous lift, as it has a very small effect (small values), the different configurations present viscous lift values of the same order of magnitude, which is not the case for the pressure lift.

Looking at the pressure drag component (Figure 8a), oscillations during the first twenty seconds have been captured until converging to a certain constant value. This behaviour is due to the unsteadiness of the simulations at the first times steps where big waves impact onto the ship's bow (wave and air velocity hit the hull's ship making big waves and smoothing them through time and iterations). In short, it can be stated that the major contribution of the pressure drag component is the wave-making resistance. Still, in the same plot, the heavily loaded conditions present a higher value than the normal loaded, and when placing the CM backward this drag gets increased (always talking in terms of absolute values). This is again related to the magnitude of the wave formation, and it's in accordance with the wave's height presented in Figure 9. Concerning the viscous drag (Figure 8b), it has been explained in Section 1.1.4 that this contribution depends on the Reynolds number (hence, velocity and characteristic length). As velocity is kept always constant, it only depends on the waterline length (thus, the wetted area). Those configurations with a higher wetted surface are the ones with larger viscous drag components. Thus, the forward heavy loaded trimming has the highest viscous drag and the centered normal loaded case has the lowest.

3.2.1 Wave-resistance component

In order to analyze the behavior of the wave-resistance component of the drag (also plotted in Figure 8a), Figure 9 shows the different waterline heights for the different cases. As commented in Section 1.1.4, the higher the wave, the bigger the drag. The bow is the most critical part in terms of wave-resistance as it is the hull's section that has to deal with "breaking" the water because of the movement of the ship. Comparing the different positions of CM, the configuration with the lowest wave generation is the centered one, as predicted. Contrasting both Loaded and Heavily Loaded configurations for the same placement of CM, not much difference can be noticed but an increase in drag for the heavier one. Lastly, a strange behavior is seen for the behind-loaded case (Figure 9a), where there is an abrupt decrease in height at the front of the ship. This is due to the fact the bulbous bow (designed to break the water and reduce

the drag) is the responsible for the generation of a notable wave at the beginning of the hull. However, in the Behind configuration, the frontal area of the hull has less contact with the water than in the other cases, decreasing the height of the wave for the first portion of the hull.

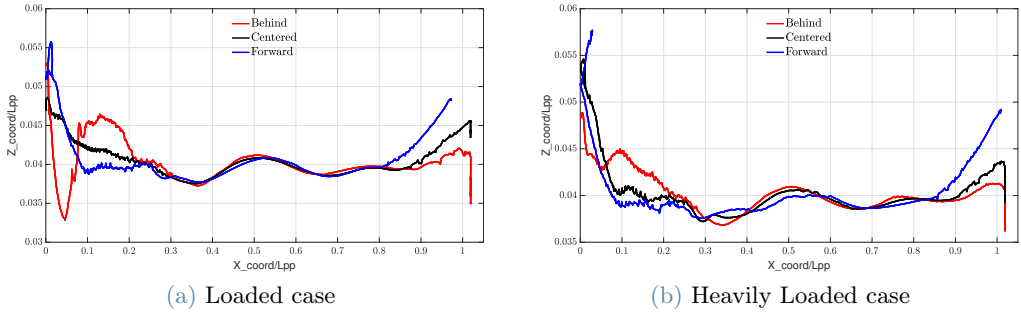


Figure 9: Waterline's height for the different cases

3.3. Flow visualization

The hull's waterline for the heavily loaded case is shown in Figure 10, where the center of mass has been moved 5% of its total length backward and forward. It can be seen that the trimming conditions for the forward case (Fig.10a) are not the optimal as the bow is way too sunken, and with a bad sea state the ship could suffer serious damage. Instead, for the backward case (Fig.10c) this trimming is not that critical, and a larger portion of the frontal area of the hull is in contact with the air.



Figure 10: Waterline visualization for different positions of the CM, with the high loaded case

In order to visualise the wave pattern of the different configurations, the dynamic pressure of the water has been computed and can be seen in Figure 11. Similar behaviour for both loaded and heavy loaded cases can be observed. The effect of the bulbous is represented as a high region of dynamic pressure for the centered and forward case. This is due to the generation of big waves when the bulbous "breaks" the water. In the behind case, this phenomenon is not much seen as the bulbous' wetted surface gets reduced. Instead, for the behind case, a high dynamic pressure in the stern region is formed. This effect is mainly due to the increased weight placed backward, which generates higher pressure gradients and it can be translated as a higher wave pattern. Both divergence and transverse wave patterns are shown as predicted in Section 1.1.4.

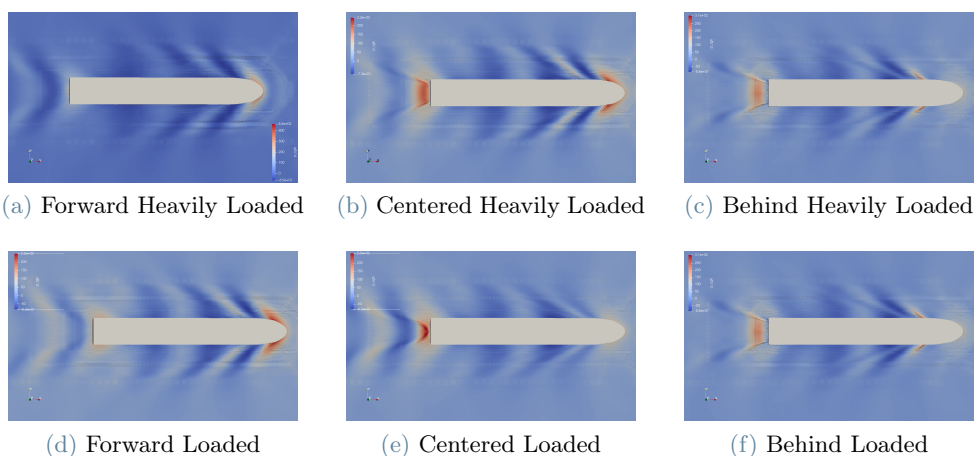


Figure 11: Dynamic pressure wave visualization in different visualizations

In Figure 12, streamlines for both water and air corresponding to the Heavy Loaded Centered condition are presented. It can be observed how the impact of both water and air on the frontal area of the hull promotes a turbulent pattern of the streamlines. This turbulent pattern is increased especially in the bulb region, since the abrupt body curvature may produce the detachment of the boundary layer. After a relaxation region, the streamlines become aligned again, for which the flow is expected to be reattached to the body. A turbulent behavior is again observed in the final portion of the hull, as it's expected since there's an abrupt change of geometry and a wake is generated behind the boat.

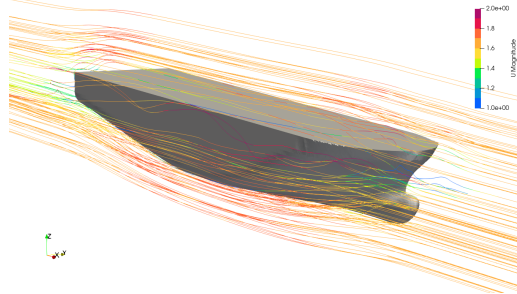


Figure 12: Water and Air streamlines

4. Conclusions

The main focus of study has been the hull's resistance behaviour while performing URANS simulations in calm conditions, for the six configurations considered. The ship resistance has been divided in two main components: viscous drag and pressure drag, but also focusing on the wave-resistance component. The buoyancy force (Lift Force) has been also computed, but bearing in mind that its effect was not the main focus of study.

The optimal configuration in terms of both dimensional drag and C_D is the Ceneterd case for both Loaded and Heavily Loaded conditions, with a $C_D = 0.0034$ and $C_D = 0.0040$ respectively. This configuration also presents the lower wetted surface for the Loaded condition. The most penalizing configuration in terms of C_D is the Forward Heavily Loaded configuration with a $C_D = 0.0054$, and it presents the largest wetted surface. The largest dimensional drag force corresponds to the Behind Heavily Loaded configuration. However, since it present a lower wetted area than the Forward Heavily Loaded case, the resulting C_D is not the most penalizing one. When decomposing the resistance into its pressure and viscous contributions, it has been observed how both contributions have a significant impact on the overall drag. However, when observing the lift force contributions, it has been observed how pressure plays a more important role than viscosity, with values up to 3 or 4 orders of magnitude higher for the pressure lift. This phenomena could be related to the low free-stream velocity considered, and it should be further studied if for larger freestream velocities the viscous contribution would have a greater impact. The wave pattern described in the theory was well captured by the simulations, and they were in accordance with the forces decomposition and wave contribution to drag.

References

- [1] V. Bertram. *Practical Ship Hydrodynamics*. Butterworth-Heinemann, 2000.
- [2] International Towing Tank Conference. *Practical Guidelines for Ship CFD Applications*. ITTC – Recommended Procedures and Guidelines, 2011.
- [3] Christopher J. Greenshields. *OpenFOAM User's Guide 5.0*. OpenFOAM Foundation Ltd, 2017.
- [4] T. Zorn. O. el Moctar, V. Shigunov. *Duisburg Test Case: Post-Panamax Container Ship for Benchmarking*. Journal of Ship Technology Research VOL.59 NO.3 PP.50-65, 2012.